The ortho to para ratio of H_2 in the starburst of NGC 253.

Andrew Harrison[1,2], Phil Puxley[3], Adrian Russell[4] and Peter Brand[1]

[1]Institute for Astronomy, University of Edinburgh, Blackford Hill, Edinburgh, UK, EH9 3HJ

[2]Present Address: Mullard Radio Astronomy Observatory, Cavendish Laboratory, Madingley Road, Cambridge, UK, CB3 0HE

[3]Gemini 8m Telescopes Project, 950 N. Cherry Ave. Tucson, Arizona, USA, 85719

[4]Astronomy Technology Centre, Royal Observatory, Blackford Hill, Edinburgh, UK, EH9 3HJ

Received ______________; accepted ______________

ABSTRACT

We present measurements of several near-IR emission lines from the nearby galaxy NGC 253. We have been able to measure 4 H_2 lines across the circumnuclear starburst from which we estimate the ortho to para ratio of excited H_2 to be ~ 2. This indicates that the bulk of the H_2 emission arises from photo-dissociation regions (PDRs), rather than from shocks. This is the case across the entire region of active star formation.

As the H_2 emission arises from PDRs, it is likely that the ratio of H_2 to Brγ is a measure of the relative geometry of O and B stars and PDRs. Towards the nucleus of NGC 253 the geometry is deduced to be tightly clustered O and B stars in a few giant HII regions which are encompassed by PDRs. Away from the nuclear region, the geometry becomes that of PDRs bathed in a relatively diffuse UV radiation field.

The rotation curves of 1-0 S(1) and Brγ suggest that the ionised gas is tracing a kinematic system different to that of the molecular gas in NGC 253, particularly away from the nucleus.

Subject headings: galaxies: ISM – galaxies: individual: (NGC 253) – galaxies: starburst

1. Introduction

1.1. How is H_2 excited in galaxy nuclei?

Molecular hydrogen makes up the bulk of the mass of molecular clouds but emission from H_2 only traces the location of energetic events within or around the clouds. The molecule's low moment of inertia means its rotational levels are well separated, with no excited levels populated in cold clouds (T $\leq$ 100 K) and so it does not radiate in quiescent clouds. The two most common processes of exciting H_2 in the ISM, particularly towards star forming regions, are thermal collisions and fluorescence.

Collisionally excited H_2 emission has been observed in a variety of Galactic sources including bipolar outflows (Fernandes 1993) and supernova remnants (Graham *et al.* 1987). Although the exact shock process is uncertain in many cases, be it C-shocks or J-shocks (see Burton 1992 for a review), the excitation of H_2 is through collisions and hence is a thermal process.

Far-UV (11-13.6 eV) photons incident upon a molecular cloud produce a photo-dissociation region (PDR) in which H_2 is fluorescently excited (Black & van Dishoeck 1987, hereafter BvD). The H_2 spectra produced by low-density PDRs (n $< 3\times10^3$ cm^{-3}) all have the same characteristic non-thermal shape with relative line intensities that are insensitive to the cloud parameters including the gas density and intensity of the incident UV radiation. This is because the intensities are determined primarily by the branching ratios of the purely radiative quadrupole ro-vibrational transitions, which are molecular constants. Observationally, this results in the line ratio of 2-1 S(1) / 1-0 S(1) being far higher in low density fluorescent regions (BvD) than it is in shocked gas (Brand *et al.* 1988). In denser PDRs the interpretation of fluorescent H_2 emission is complicated by the need to consider collisional de-excitation of the H_2 molecule, mainly through collisions with H atoms (Sternberg & Dalgarno 1989). The spectrum is modified as the levels are pushed toward local thermodynamic equilibrium (LTE) and can resemble the thermal spectrum seen in shocks. Observationally, this results in the 2-1 S(1) / 1-0 S(1) line ratio being similar in both dense PDRs and shocked gas (Burton *et al.* 1990). It is still possible to discriminate between shocks and dense PDRs by observing transitions from the higher energy transitions, such as 3-2 S(4), because these levels only have significant populations in PDRs. Unfortunately, these high energy transitions are very weak and so need particularly sensitive observations to detect them. In extragalactic studies, detection of these weak lines is difficult in practice, due to the intrinsic uncertainty in the spectrum of the underlying continuum.

Due to the difficulties of discriminating between dense PDRs and shocks there is currently no consensus of what is the dominant excitation mechanism of H_2 in external galaxies. Observations of Galactic PDRs indicate that the ortho/para ratio of excited H_2 is around 2 and not the hot thermal limit of 3 (Chrysostomou *et al.* 1993). In section 4.1, we show that the observed ortho to para ratio of H_2 is a clear discriminant between fluorescent and shock excitation of H_2 in starburst galaxies.

Once the dominant excitation mechanism of H_2 is determined comparison of H_2 measurements with observations of other tracers enables modelling of the physical processes in a starburst. In particular, K-window spectra of galaxies show the bright hydrogen recombination line, Brγ. This line will arise from regions in which hydrogen is predominantly ionised, *i.e.* HII regions. In recent years, mainly because of the uncertainty over the dominant excitation mechanism of H_2 in galaxy nuclei, there has been a debate over what is traced by the ratio of 1-0 S(1) to Brγ. Lester *et al.* (1990) suggested that radial variations in the ratio of shocks to PDRs within starbursts resulted in variations in the 1-0 S(1) / Brγ ratio. An alternative picture has been proposed by Puxley, Hawarden & Mountain (1990), hereafter PHM, who suggested that the efficiency with which PDRs turn far-UV photons into IR H_2 emission is responsible for the scatter in the ratio of 1-0 S(1) / Brγ.

To test whether the ortho/para ratio of H_2 could be measured in a starburst nucleus, and hence be used to determination of the principal excitation mechanism of H_2, the circum-nuclear region of NGC 253 was observed.

1.2. NGC 253

The Sculptor galaxy NGC 253, a highly inclined spiral (i=78°, Pence 1981) of type Sc(s) (Sandage & Bedke 1995), is perhaps the best example of a nearby nuclear starburst (Rieke *et al.* 1988). Mauersberger *et al.* (1996) reviewed the published distance estimates for NGC 253. The distance we have adopted is 2.75 Mpc.

NGC 253 is among the most prominent extra-galactic sources, showing emission characteristic of starburst activity from the radio range, *e.g.* Ulvestad & Antonucci (1991), to the infrared, *e.g.* Telesco *et al.* (1993), to X-rays, *e.g.* Fabbiano & Trinchieri (1984). This emission is believed to be starburst in origin, rather than from an Active Galactic Nucleus (AGN), because: the X-ray emission is from extended diffuse gas, rather than from a point source (Fabbiano & Trinchieri 1984); radio images show many sources in the nucleus rather than just a point source (Ulvestad & Antonucci 1991); there are no large line widths; there are no high-excitation near-IR lines and the CO depth looks stellar, which suggests that there is no AGN continuum dilution.

The starburst in NGC 253 was presumably triggered by a bar potential (Scoville *et al.* 1985, Canzian *et al.* 1988). The starburst is centrally concentrated, covering a region of size of only about one hundred parsecs ($\sim 8''$, Telesco *et al.* 1993). The bolometric luminosity of the starburst is generated by a population of massive stars still undergoing nucleosynthesis. The luminosity is not generated by supernova (SN) remnants because the derived SN rate of ≤ 0.25 yr^{-1} (Ulvestad & Antonucci 1991) accounts for less than 20% of the total luminosity.

NGC 253 contains molecular gas that is both warm and dense (Harris *et al.* 1991). The far-IR and sub-mm emission from NGC 253 is consistent with the molecular gas being principally excited through UV photons, rather than through shocks (Carral *et al.* 1994, Harrison *et al.* 1995, Harrison 1996). The interpretation of the near-IR H_2 emission is more controversial, with PHM favouring UV excitation whereas Rieke *et al.* (1988) suggest that shocks are responsible.

2. Observations and data reduction

K band spectra of the circum-nuclear region of NGC 253 were observed on the nights of 19-21 November 1993 with the United Kingdom Infrared Telescope (UKIRT) on Mauna Kea, Hawaii. The instrument used was the cooled grating spectrometer, CGS4, which had a long slit ($90''$) projected onto a 62×58 pixel InSb array (Mountain *et al.* 1990). In the configuration employed, the instrument had a spatial resolution of $3''$ per pixel which resulted in only the middle 30 rows of the array being illuminated. The width of the slit was also $3''$. The angle of the slit was fixed at $51°$ east of north so that the slit was placed along the major axis of NGC 253. The central position of NGC 253 was chosen to be R.A.(B1950) $0^h\ 45^m\ 5.76^s$, Dec. $-25°\ 33'\ 36.0''$.

We observed 4 distinct wavelength bands within the K window in order to get higher spectral resolution than a single band covering the entire K window. The sub-bands observed covered the wavelength regions: 1.98-2.08μm; 2.06-2.16μm; 2.14-2.24μm; 2.22-2.32μm. The spectral dispersion of the sub-bands, measured from a calibration spectrum of an an argon lamp, was 107 km s^{-1} pixel^{-1} and the velocity resolution was 220 km s^{-1} at 2.2μm ($R = \lambda/\Delta\lambda \approx 1350$).

We also took lower resolution spectra of the K window, in order to normalise the absolute fluxes of the individual high resolution spectra. The low resolution spectra had a spectral dispersion of 454 km s^{-1} pixel^{-1} and velocity resolution of 980 km s^{-1} at 2.2μm ($R = \lambda/\Delta\lambda \approx 300$).

The observations were sampled spectrally by moving the detector by half a pixel over 2 pixels giving integrations at 4 detector positions. This mode of sampling, *i.e.* over 2 pixels, was used so as to minimise the effects of bad pixels on the array (Puxley *et al.* 1992). The data were reduced in the usual way, *e.g.* Harrison (1996). The wavelength scales of the spectra were calibrated by making observations of the known transitions from either an argon or krypton lamp. Flux calibration was carried out by making observations of the standard star HR 12 (spectral type = A3V, $m_k = 5.74$).

2.1. Normalising and overlapping the spectra

Each of the separate high-resolution data was normalised to the relevant wavelength region in the low resolution spectrum by multiplication of the flux, to correct for small pointing errors, and differences in seeing, between the sub-band observations.

Once the spectra from each sub-band were normalised, they were combined through a weighted mean to produce a final sub-spectrum. Each of the separate sub-spectra were then joined together by choosing a reasonable overlap region and taking the weighted mean of the points within this region. We now had a complete high resolution spectrum of the entire wavelength region 2.02μm $\rightarrow$ 2.31μm. Figure 1 shows the nuclear spectrum. This spectrum has a signal to noise ratio of $\sim$ 400 per pixel. All the features in the continuum in Figure 1 are real, caused by absorption lines in the atmospheres of cool stars.

2.2. Measuring emission lines in the K band spectra of NGC 253

To measure the emission lines of interest it is important to model the continuum, as several absorption features coincide in wavelength with emission lines produced in the ISM. The technique that was applied to do this is discussed in detail in Harrison (1996) and is summarised below.

Kleinmann & Hall (1986), hereafter KH, produced an atlas of K band spectra of various stars. It was decided to use the CO (2,0) band-head, at 2.3 μm, that is also apparent in the spectra of NGC 253, to attempt to simulate various admixtures of stellar populations and non-stellar emission. We chose 8 different stars from the KH atlas, listed in Table 1, which covered the range of stars that may exist in all or part of the nuclear region and which could feasibly dominate the emission. Inspection of these stars revealed that the spectra of NGC 253 are flatter than all the KH stars and, furthermore, the CO band-head in NGC 253 is weaker than the giant and supergiant KH stars. Therefore, there has to be a component to the overall luminosity in the K window that is not stellar and both fills in the CO band-head and makes the spectra flatter. Such an extra component is likely to be warm/hot dust with T $\sim$ 600-1000 K, as suggested by Scoville *et al.* (1985). Dust is likely to be responsible, rather than other emission mechanisms (Puxley 1991).

It is difficult to constrain the relative contribution of stars, dust, free-free emission and extinction at any point because of the uncertainties in the temperature and emissivity of the dust and the population of stars. Rather than separate all the various contributions to the continuum emission, we simulated the addition of all the components as follows. We first corrected the stellar spectrum for the recessional velocity of NGC 253, via the CO band-head. We then normalised the stellar CO depth to that of NGC 253 by adding a constant and multiplying by a constant to the flux. The slope of the corrected KH star was then corrected by a 2nd order polynomial so that it matched the observed slope of NGC 253. Figure 2 shows that this technique produces an accurate match between adjusted KH stars and the spectrum of NGC 253.

To measure the ortho/para ratio we used the 3 brightest emission lines of H_2 in our spectra, 1-0 S(2) (at 2.04μm), 1-0 S(1) (at 2.13μm) and 1-0 S(0) (at 2.22μm). For each line at each spatial position we subtracted one of the eight fitted KH stars from the local continuum. The residuals left by the subtraction were then fitted with an arbitrary polynomial so as to model the true continuum under the line. The resulting emission line was then fitted with a Gaussian in order to measure the flux, centroid and FWHM of the line. The same approach was applied to each of the other 7 KH stars. This gave 8 different measurements of each line at each position. We used the average and the standard deviation of the eight different values as the estimates of the flux, centroid and the FWHM of the lines and the respective uncertainty in these values.

The energy levels of the three H_2 transitions are sufficiently similar that the emission of all three lines should be coextensive. Thus, the FWHM of these lines should also be very similar. Furthermore, these three lines should all have the same Doppler-shifted recessional velocity. Therefore, if a choice of parameters in the continuum subtraction resulted in one of the three lines having a FWHM or velocity centroid that differed noticeably from the other two lines then it was assumed that this was due to the continuum subtraction introducing an unwanted systematic error into the wayward line's measurements. Iteratively adjusting the continuum subtraction parameters of the wayward line, such as wavelength region fitted or polynomial order, eventually resulted in a closer match between the Doppler-shift and FWHM of the three lines.

Measuring the 2-1 S(1) line (at 2.25 μm) allows the determination of the vibrational temperature by comparing this line with the 1-0 S(1) line. Moreover, the ratio of these two lines has been used in the past as evidence that the H_2 is excited in either shocks or PDRs. The wavelength of the line coincides with a calcium absorption feature and so to measure the line accurately it is important to reliably subtract the local continuum. By carrying out a similar analysis to that used to measure the 3 H_2 lines from the v = 1-0 series, it was found that the FWHM of the 2-1 S(1) is less than the FWHM of the v = 1-0 lines. The fact that the FWHM of the 1-0 S(1) is different to that of 2-1 S(1) means that the emission cannot be entirely coextensive.

2.3. What are the likely errors in the measurements?

Each of the high-resolution spectra from different nights have variations in the "calibrated" flux of up to 40%, caused by aggregate pointing and seeing variations. The systematic error introduced by combining these spectra is less than 40% because we have a measure, through the low resolution spectra, of the absolute flux for each position. It is estimated that combining spectra covering the same wavelength region, but observed on different nights, will result in a systematic uncertainty of $\leq$ 10% in the flux of the line of interest. In the overlap region, between two adjoining spectra covering different wavelengths, the weighted mean of the two spectra was used to produce the "true" spectrum. It is estimated that this technique could cause systematic uncertainties in the flux in the overlap regions of $\leq$ 10%. The only line that falls in one of the overlap regions is 1-0 S(0), at 2.225μm. The statistical errors in our spectra are considerably smaller than the photometric uncertainty.

3. Results of H_2 measurements and their implications

Table 2 lists all the measured fluxes of lines towards NGC 253 and Table 3 lists the relevant line parameters of the H_2 lines. Figure 3 illustrates the column densities observed at the nuclear position.

Although we have only measured 4 lines it is possible to constrain the excitation mechanism of H_2. The rotational temperature can be determined using 1-0 S(2) and 1-0 S(0); the vibrational temperature can be determined using 1-0 S(1) and 2-1 S(1); the ortho/para ratio of H_2 can be determined using 1-0 S(2), 1-0 S(1) and 1-0 S(0). Details are given in the appendix.

Figure 4 shows the rotational and vibrational temperatures. The rotational temperatures are $\sim$ 1000 K and the vibrational temperatures are $\sim$ 3000 K at all of the observed positions, indicating that the same excitation process is responsible for the H_2 emission.

Figure 5 shows the ortho/para ratios measured from the v = 1 lines across the galaxy. The values are around 2 everywhere, and nowhere is it measured to be 3 within the errors. This ratio does not vary, confirming that the principal excitation process of H_2 is the same across the starburst.

Figure 6 shows how the ratio of molecular hydrogen emission to ionised hydrogen emission varies. This profile is consistent with a similar plot of the 1-0 S(1) / Brγ ratio in NGC 253 reported by Prada *et al.* (1996). The U-shaped structure, with a minimum in the 1-0 S(1) / Brγ ratio near the nucleus, has been observed in similar analyses of several other galaxies, notably M82 and NGC 4945 (Prada *et al.* 1996). Lester *et al.* (1990) argued that the rise in the 1-0 S(1) / Brγ ratio towards the molecular ring of M82 implied that molecular gas was being shocked in the ring of gas around the starburst, as such shocks would generate H_2 emission but little Brγ. PHM proposed an alternative model in which the efficiency with which PDRs transform far-UV photons into IR H_2 emission is responsible for the observed change in the ratio of 1-0 S(1) / Brγ.

We show in the following section that the data presented in this paper demonstrate conclusively that the emission of H_2 in NGC 253 is by fluorescence and that a shock contribution, if any, must be small. In these circumstances, we show that this allows an interpretation of 1-0 S(1) / Brγ in terms of the models of starbursts outlined by PHM.

4. Discussion

4.1. The ortho/para ratio $\sim$ 2 means fluorescence

It is believed that H_2 is formed on dust grains. The ortho/para ratio may take any value, depending on the yet unknown formation mechanism. The picture is further complicated because the molecule may remain on the grain for some time before being ejected into the gas and will be thermalised at the lower temperature of the grain (Chrysostomou *et al.* 1993). Once the ortho/para ratio is determined conversion between the two states occurs in the gas phase by spin exchange reactions with H and H^+ (Takayanagi *et al.* 1987) or with excited H_2 (Willacy, private communication). Conversion between the two states via radiative or collisional transitions is very inefficient. At high temperatures, above a few hundred K, with spin exchange permitted, the ortho/para ratio would become equal to the ratio of spin degeneracy, *i.e.* 3. This is the value observed in shocked H_2 emission (Brand *et al.* 1988).

In PDRs the observed values of the ortho/para ratio range from 1.7 to 2.3, *e.g.* Chrysostomou *et al.* (1993) and Ramsay *et al.* (1993). Such values have been explained in several ways and may indicate that H_2 is formed at a low temperature on dust (Takayanagi *et al.* 1987) or that the ortho- and para- H_2 self-shield at different depths into a PDR (BvD).

As we measure the ortho/para ratio to be $\sim$ 2 at all observed positions in NGC 253 this shows that fluorescence is responsible for producing the bulk of the H_2 emission, at all positions within the starburst.

4.2. The efficiency with which far-UV is turned into H_2 IR emission

The efficiency, η, with which the UV flux impinging upon a molecular cloud, I_{UV}, is converted into a flux of IR photons, I_{IR}, has been discussed in detail by several groups (BvD, Burton, Hollenbach & Tielens 1990 and Sternberg 1988). For a given density of the gas, I_{IR} initially increases almost linearly with increasing I_{UV} but eventually saturates at some asymptotic value. This limit to fluorescent emission results from the competition between grains and molecules for absorbing the ultraviolet photons. If H_2 absorbs all the incoming UV photons then H_2 will be excited at maximum efficiency. If the dust becomes optically thick to the UV before H_2 goes optically thick then an increase in the UV field or density will not result in a larger column of excited molecular hydrogen. The depth into the cloud at which dust becomes optically thick to UV is fixed at a specific column density of gas whereas the depth into the cloud at which H_2 becomes optically thick depends primarily on ratio of the intensity of the incident ultraviolet radiation[1], χ, and the gas density, $n = 2n_{H_2} + n_H$. The efficiency of H_2 excitation is maximised for small χ/n, when the attenuation of UV radiation is dominated by line absorption (BvD). In this regime all the incoming UV photons dissociate and excite H_2. For larger values of χ/n (units cm^3), the efficiency is reduced because of the removal of UV photons by dust. PHM concluded that the extent to which the stellar radiation is diluted by geometry is pivotal in determining the relation between the molecular hydrogen luminosity and the UV luminosity from a starburst.

4.3. The radial variation of 1-0 S(1) / Brγ as a measure of OB clustering in NGC 253

PHM explored 3 scenarios for the different geometries between the HII regions and PDRs and show that the geometry is crucial in determining the emitted 1-0 S(1) / Brγ ratio. A ratio less than 0.4, as observed towards the nucleus of NGC 253 (Figure 6), implies that $\chi/n > 1$. That is, there is an intense UV field or low gas density. Harrison *et al.* (1995) argue that the gas density is likely to be greater than 10^4 cm^{-3} in the nucleus, *i.e.* not low. This in turn implies that the 1-0 S(1) / Brγ ratio is low because the UV intensity is high in the nuclear region. PHM suggested that such a high UV intensity could be readily generated by a large cluster of OB stars.

If we assume that the nuclear OB cluster resides within a common Strömgren sphere which the molecular gas envelops, then it is straightforward to estimate the UV intensity, χ, impinging upon the PDR. The ionising photons produce ionisations/recombinations throughout the volume of the HII region whereas PDR emission arise from the surface of the volume. Moreover, PHM noted that if the OB stars are tightly grouped near the centre of the HII region then the relative ionising and nonionising UV photon fluxes can be characterised by an effective temperature (T_{eff}) set by the stellar mass function. Towards the nucleus of NGC 253, Carral *et al.* (1994) estimated that the electron density in the ionised gas is 430 cm^{-3} and the electron temperature is 8000 K. Using

[1] χ is the 91.2-110.8 nm photon flux per unit surface area relative to the mean starlight background in the solar neighbourhood: 2.0×10^{11} photon s^{-1} m^{-2}. The χ quoted is from the Draine (1978) radiation field, not the value of Roberge, Dalgarno & Flannery (1981)—see BvD for further details. The level of OB clustering results in the scaling between the UV energy density and χ impinging upon PDRs.

these values, and the total recombination coefficient (Dyson & Williams 1980), the intensity of the UV radiation at the edge of the Strömgren sphere is

$$\chi = 5.8 \times 10^{-14} \Theta(T_{eff}) \left(\frac{N_{Lyc}}{s^{-1}}\right)^{1/3} R^{-2} \tag{1}$$

where $\Theta(T_{eff})$ is the ratio of nonionising to ionising photon fluxes, N_{Lyc} is the ionising photon flux and R is a dimensionless cloud-radiation source separation in units of the Strömgren radius. PHM have tabulated $\Theta(T_{eff})$ for various IMFs and the corresponding effective temperatures. From the central three pixels we measure the average flux of Brγ to be $\sim 1 \times 10^{-16}$ W m^{-2}, with the main uncertainties resulting from how much the observed flux is reduced by extinction. The Hummer & Storey (1987) recombination coefficients for electron densities of 10^{2-3} cm^{-3} and T_e = 7500 K show that every 64 Lyman continuum photons result in 1 Brγ photon. Hence, the number of Lyman continuum photons generated in the nuclear region of NGC 253, N_{Lyc}, is $\sim 1 \times 10^{52}$ s^{-1}. Carral *et al.* (1994) suggest that the effective temperature in NGC 253 is 35,000 K. PHM calculate Θ(35,000 K) $\simeq$ 2. Thus we find the average UV flux impinging upon the PDR surrounding the cluster is $\chi \approx 2.2 \times 10^4$.

PHM also considered the scenario in which individual stars are surrounded by their own Strömgren spheres, Each star has its own associated PDR and because each star produces a much smaller number of Lyman continuum photons than a cluster, the intensity of radiation at the Strömgren sphere is less. PHM tabulated the N_{NUV}, *i.e.* the non-ionising UV photon flux in the range 91.2-110.8 nm, and N_{Lyc} photon fluxes for different stars. For a star with an effective temperature of 35,000 K the number of Lyman continuum photons per second is $10^{48.34}$ and the number of UV photons per second is $10^{48.60}$. Thus, the average UV flux expected at the edge of each individual Strömgren sphere is $\chi \approx 1400$.

Notwithstanding the uncertainties concerning extinction corrections, IMF and the exact geometry it appears that χ is greater than 10^3. The calculations of PHM suggest that a low ratio of 1-0 S(1) / Brγ in high density molecular gas is most easily achieved if the geometry is that of giant OB clusters surrounded by large PDRs, rather than that of individual OB stars surrounded by their own individual PDRs. Therefore, it is likely that χ is at least 10^4 within the active part of the starburst.

The ratio of 1-0 S(1) / Brγ in NGC 253 shows a rise with galactocentric radius, Figure 6, and shows values approaching 10 towards the edge of the region observed. PHM argued that the most likely geometries of regions exhibiting 1-0 S(1) / Brγ ratios of these values are PDRs that are bathed in a relatively diffuse field. In the case of diffuse ultraviolet radiation, the UV-to-IR conversion efficiency tends to a maximum value. The efficiency becomes independent of the gas density provided that χ/n $\ll$ 0.1.

Summarising, the H_2 emission from NGC 253 is produced entirely by PDRs. That is, the rise in the 1-0 S(1) / Brγ ratio, with galactocentric radius, does not arise from a change in the ratio of shocks to PDRs. Furthermore, the observed ratio of 1-0 S(1) / Brγ suggests that towards the nucleus of NGC 253, OB stars have to be clustered so as to produce a high UV field impinging upon the PDRs. Away from the nuclear region the UV field is relatively low. It is uncertain whether the diffuse radiation field, away from the nucleus, is leaking from the active starburst or whether it is produced locally.

4.4. Other evidence for the clustering of star formation in the circumnuclear region of NGC 253

Observations made at radio wavelengths show a population of luminous flat radio sources across the nucleus of NGC 253 (Ulvestad & Antonucci 1991). If these are HII regions, then their brightness indicates that each one must contain many hundreds, possibly thousands, of OB stars (Paglione *et al.* 1995). Images of NGC 253 in the IR show one particular strong emitter that is located at, within pointing errors, a flat spectrum source (Sams *et al.* 1994, Piña *et al.* 1992 and Keto *et al.* 1993). This particular source appears to have a bolometric luminosity of $\sim 2\times10^{9}$ $L_{\odot}$, generated by a cluster of stars with a half-light radius of ≤ 3 pc (Watson *et al.* 1996). HST images also show several other young clusters in the starburst, which are less luminous than the main cluster (Watson *et al.* 1996). The HST clusters spatially coincide with several of the near-IR peaks (Sams *et al.* 1994) although it appears that some of the clusters may be spatially offset from the flat radio sources, probably due to source confusion in the radio images, pointing offsets in the optical and IR images, and extinction.

4.5. The kinematics of the ionised and molecular gas in NGC 253

Figure 7 shows the position/velocity diagram of ionised gas, traced by Brγ, compared with the PDR gas, traced by 1-0 S(1). As can be seen there is an apparent difference between the two tracers indicating that as we travel away from the nucleus the contributing HII regions and PDRs are not coexistent in velocity space. The difference in kinematics ($\sim$ 50 km/s) between the Brγ and 1-0 S(1) is consistent with the work of Prada *et al.* (1996).

A physical separation between the young stars and nearby molecular gas will dilute the radiation field impinging upon PDRs. This diluted radiation field will then enhance the observed 1-0 S(1) / Brγ ratio towards the edge of the starburst region. Alternatively, the radial increase in the ratio may mean that the starburst age increases towards the edge, with less hard UV photons further out. If this is the case, then the older population of star-forming regions has a different distribution to the younger generation and so will sample a different set of positions on the position-velocity diagram. A further explanation of the radial change in the 1-0 S(1) / Brγ ratio is that the upper end of the initial mass function, either the slope or the largest stellar mass produced, is decreasing radially, again resulting in a decrease of hard UV photons towards the edge of the starburst.

5. Conclusions

In this paper we have presented measurements of several near-IR emission lines from NGC 253. In particular, we have been able to measure 4 H_2 lines across the starburst which has allowed an estimate of the ortho to para ratio of H_2. The ratio is observed to be close to 2, and not 3, which indicates that the bulk of the H_2 emission arises in PDRs rather than shocks. This is the case across the entire starburst. We suggest that this method of determination is better than the use of the classical H_2 line ratios (1-0 S(1),1-0 S(0),2-1 S(1)).

As the H_2 emission arises from PDRs, it is likely that the ratio of 1-0 S(1) to Brγ is a measure of the geometry of OB stars to PDRs, as originally suggested by PHM. Towards the nucleus of NGC 253 the geometry is tightly clustered OB stars in a few giant HII regions which are encompassed by PDRs. The UV flux impinging upon the nuclear PDRs is high, $> 10^4$ times the local value. Away from the nuclear region, the geometry becomes that of PDRs bathed in a relatively diffuse UV radiation field.

The rotation curves of H_2 and Brγ suggest that the ionised gas is tracing a different kinematic system to that of the molecular gas, particularly away from the nucleus where it is likely that the PDRs are bathed in a relatively low UV field.

6. Acknowledgements

We would like to thank Henry Buckley, Bob Joseph, Mike McCartney, Steve McNally, Suzie Ramsay, Milagros Ruiz, Ewine van Dishoeck and Karen Willacy for their helpful and patient discussions. AH would also like to thank both PPARC, for providing a studentship, and the Benefits Agency, who unwittingly stepped in to replace PPARC in providing financial aid.

7. References:

Black J. & van Dishoeck E. 1987, ApJ, 322, 412 (BvD)

Brand P., Moorhouse A., Burton M., Geballe T., Bird M. & Wade R. 1988, ApJ Lett., 334, L103

Burton M. 1992, Aust. J. Phys., 45, 463

Burton M., Hollenbach D. & Tielens A. 1990, ApJ, 365, 620

Canzian B., Mundy L. & Scoville N. 1988, ApJ, 333, 157

Carral P., Hollenbach D., Lord S., Colgan S., Haas M., Rubin R. & Erickson E. 1994 ApJ, 423, 223

Chrysostomou A., Brand P., Burton M. & Moorhouse A. 1993, MNRAS, 265, 329

Draine B. 1978, ApJ Supp., 36, 595

Dyson J. & Williams D. "The physics of the interstellar medium", 1980, Manchester University Press

Fabbiano G. & Trinchieri G. 1984, ApJ, 286, 491

Fernandes A., 1993, PhD Thesis, University of Edinburgh

Graham J., Wright G. & Longmore A. 1987, ApJ, 313, 847

Harris A., Hills R., Stutzki J., Graf U., Russell A. & Genzel R. 1991, ApJ Lett., 382, L75

Harrison A. 1996, PhD Thesis, University of Edinburgh

Harrison A., Puxley P., Russell A. & Brand P. 1995, MNRAS, 277, 413

Hummer D. & Storey P. 1987, MNRAS, 224, 801

Keto E., Ball R., Arens J., Jernighan G., Meixner M., Skinner C. & Graham J. 1993, ApJ Lett., 413, L23

Kleinmann S. & Hall D. 1986, ApJ Supp., 62, 501 (KH)

Lester D., Carr J., Joy M. & Gaffney N. 1990, ApJ, 352, 544

Mauersberger R., Henkel C., Wielebinski R., Wilkind T. & Reuter H. 1996, A&A, 305, 421

Mountain C., Robertson D., Lee T. & Wade R. (1990), in Crawford D. ed., Proc. SPIE 1235, Instrumentation in Astronomy VII., Bellingham, p.25

Paglione T., Tosaki T. & Jackson J. 1995, ApJ Lett., 454, L117

Pence W. 1981, ApJ, 247, 473

Piña R., Jones B & Puetter R. 1992, ApJ Lett., 401, L75

Prada F., Manchado A., Canzian B., Peletier R., McKeith C. & Beckman J. 1996, ApJ, 458, 537

Puxley P. 1991, MNRAS, 249, 11P

Puxley P., Beard S. & Ramsay S. (1992), in Grosbøl P., de Ruijsscher R. eds, ESO Conf. Proc. 41, 4th ESO/ST-ECF Data Analysis Workshop, ESO, Garching, p.117

Puxley P., Hawarden T. & Mountain M. 1990, ApJ, 364, 77 (PHM)

Ramsay S., Chrysostomou A., Geballe T., Brand P. & Mountain M. 1993, MNRAS, 263, 695

Rieke G., Lebofsky M. & Walker C. 1988, ApJ, 325, 679

Roberge W., Dalgarno A. & Flannery B. 1981, ApJ, 243, 817

Sams B., Genzel R., Eckart A., Tacconi-Garman L. & Hofmann R. 1994, ApJ Lett., 430, L33

Sandage A. & Bedke J. 1995, The Carnegie Atlas of Galaxies

Scoville N., Soifer B., Neugebauer G., Young J., Mathews K. & Yerka K. 1985, ApJ, 289, 129

Sternberg A. 1988, ApJ, 332, 400

Sternberg A. & Dalgarno A. 1989, ApJ, 338, 197

Takayanagi K., Sakimoto K. & Onda K. 1987, ApJ Lett., 318, L81

Telesco C., Dressel L. & Wolstencroft R. 1993, ApJ, 414, 120

Ulvestad J. & Antonucci R. 1991, AJ, 102, 875

Watson A., Gallagher III J., Holtzmann J., Hester J., Mould J., Ballester G., Burrows C., Casertano S., Clarke J., Crisp D., Evans R., Griffiths R., Hoessel J., Scowen P., Stapelfeldt K., Trauger J. & Westphal J. 1996, AJ, 112, 534

A. Measuring the ortho to para ratio of molecular hydrogen

From the intensity ratio of any two transitions it is possible to derive an excitation temperature. One can hope to characterise the nature of the H_2 emission by deriving the excitation temperatures between different rotational and vibrational levels, T_{rot} and T_{vib}. To calculate rotational or vibrational excitation temperatures the following conditions must be met: i) for a rotational excitation temperature, the two transitions must have the same upper vibrational level and different upper and lower rotational levels, *i.e.* $\Delta v = 0$ $\Delta J \neq 0$; ii) for a vibrational excitation temperature, the two transitions must have different upper and lower vibrational levels and the same rotational level, *i.e.* $\Delta v \neq 0$ $\Delta J = 0$

It is thus possible to derive a rotational temperature using the transitions 1-0 S(1) and 1-0 S(0), and to derive a vibrational temperature using the transitions 1-0 S(1) and 2-1 S(1). There is a difference in these temperature measures between the shock and PDR case. In the shocked case, the derived rotational temperature is close to the derived vibrational temperature, as would be expected from gas in LTE. Contrary to this is the PDR case where the derived rotational temperature is much lower than the derived vibrational temperature. The reason for this is that, by its nature, the fluorescent process is non-thermal. The radiative cascade induced by UV photons overpopulates the highest energy levels with respect to a Maxwell-Boltzmann population. It is this overpopulation which gives the measured vibrational temperature in a PDR to be $\sim$ 5000 K whereas the kinetic temperature of the gas is $\sim$ 10% of this (Sternberg & Dalgarno 1989).

In the preceding discussion we have argued that the ratio of the 1-0 S(1) and 1-0 S(0) transitions can be used to measure a rotational temperature. The 1-0 S(0) line is a transition between two para states and the 1-0 S(1) line is a transition between two ortho states. The normalisation of the levels implicitly assumes that the ortho to para ratio of H_2 is equal to three, the high temperature limit. However, in most PDRs the observed ortho to para ratio is less than 3 (Chrysostomou *et al.* 1993). From measured H_2 line intensities it is possible to calculate the ortho to para ratio. The rotational excitation temperatures for each vibrational level are calculated using two levels with the same spin to accommodate our initial ignorance of the ortho to para ratio. Ratioing two transitions from separate ortho and para states then allows the ortho to para ratio to be calculated. However, care must be taken because the rotational excitation temperature changes with J; it gets higher with increasing J. To cater for this fact it is best to calculate the ortho to para ratio with the level which is straddled by the levels used to calculate the rotational excitation temperature. For instance, for v = 2, the 2-1 S(0) and 2-1 S(2) transitions can be used to calculate the rotational excitation temperature, and to calculate the ortho to para ratio the 2-1 S(0) and 2-1 S(1) transitions would be used.

The degeneracy for each level is $g_j = g_s g_J$, where g_J is the rotational degeneracy given by $g_J = 2J + 1$. Leaving the spin degeneracies for the ortho and para states as free parameters, the ortho to para ratio is calculated with the equation

$$\frac{g_s^O}{g_s^P} = \frac{(2J_P+1)}{(2J_O+1)} \frac{I_O \lambda_O A_P}{I_P \lambda_P A_O} exp\left(\frac{-\Delta E}{kT_{rot}}\right) \tag{A1}$$

where g_s^O, g_s^P = spin degeneracies for ortho and para states; J_O, J_P = rotational quantum number for ortho and para states; I_O, I_P = intensity of ortho and para transitions; A_O, A_P = spontaneous radiative decay probability of ortho and para transitions; ΔE = energy difference between the para and ortho states.

Figure captions

- Figure 1: High-resolution spectrum at the nuclear position of NGC 253 showing the features we discuss in the paper. One σ error bars are displayed for each of the pixels.

- Figure 2: The modified KH standard SU Per overlaid on the nuclear spectrum of NGC 253. Note the good match between the stellar absorption features and the galaxy continuum.

- Figure 3: The column density diagram for the nuclear position. The rotational temperature is derived from a comparison of the column densities in the 1-0 S(2) and 1-0 S(1) transitions. The vibrational temperature is derived from a comparison of the column densities in the 1-0 S(1) and 2-1 S(1) transitions. The ortho/para ratio is derived from a comparison of the column density in the 1-0 S(1) line with the value predicted through a comparison of the 1-0 S(0) and 1-0 S(2) lines.

- Figure 4: The rotational and vibrational temperatures across the starburst. Positive radii are in the direction of SW.

- Figure 5: The ortho to para ratios across the starburst. The value is fairly constant at all positions suggesting that the excitation mechanism is the same throughout the inner regions of NGC 253. The derived ratio of $\sim$ 2, not 3, indicates that the H_2 emission arises from PDRs, not from shocked gas. As can be seen, the systematic error in the ortho/para ratio, resulting from the combination of adjoining spectra, dominates over the random errors, resulting from the photometric uncertainty of the pixels in the spectra and the subtraction of the underlying continuum around each of the lines.

- Figure 6: The ratio of 1-0 S(1) / BrG across the starburst.

- Figure 7: The velocity of 1-0 S(1) and Brγ across the starburst. The plot is consistent with a similar plot shown in Prada *et al.* (1996).

Table 1: Stellar types chosen from the Kleinmann & Hall (1986) atlas

Star	Spectral type
SU Per	M3-M4 Iab
R Lyr	M5 III
SW Vir	M7 III
χ Peg	M2 III
BK Vir	M7 - III
γ Dra	K5 III
HR 8726	K5 Ib
μ Cep	M2 Ia

Table 2: The fluxes measured for all the positions (in units of 10^{-19} W m^{-2}).

Position along slit		1-0 S(2)	1-0 S(1)	1-0 S(0)	2-1 S(1)	Brγ
(arcsecs)[a]	(parsecs)[b]					
+21	+280	20.2±1.3[c]	48.5±2.0	17.2±1.1	—	—
+18	+240	41.6±2.1	60.7±2.0	19.1±0.9	—	9.1±0.4
+15	+200	30.6±1.8	51.6±2.0	20.4±1.2	—	7.1±0.3
+12	+160	31.4±1.6	62.4±2.0	23.9±1.2	12.4±1.2	19.0±0.7
+9	+120	50.1±1.5	128.1±2.0	51.9±1.5	22.7±1.1	55.6±1.6
+6	+80	93.1±2.3	196.7±2.1	74.5±1.8	34.4±1.1	291.9±4.9
+3	+40	127.4±6.7	299.1±2.2	125.4±3.3	74.4±1.6	1408.9±9.9
0	0	127.1±4.0	340.9±2.1	130.0±2.9	68.8±1.3	1150.0±7.5
-3	-40	101.7±2.3	236.2±2.1	88.2±2.0	39.8±1.2	484.6±4.2
-6	-80	52.4±1.9	145.3±2.3	54.8±1.7	31.6±1.5	269.3±3.9
-9	-120	38.9±1.3	98.5±2.1	38.2±1.4	19.2±1.2	103.0±2.2
-12	-160	24.1±1.4	58.5±2.0	23.7±1.3	17.3±1.8	40.4±1.5
-15	-200	20.4±2.1	30.3±2.0	13.1±1.3	—	24.0±1.6
-18	-240	14.0±2.3	20.1±2.0	9.8±1.5	—	10.5±1.1

[a]+ve values are to the SW, −ve values are to the NE

[b]$3''$=40 pc when NGC 253 is at a distance of ~2.75 Mpc.

[c]All the quoted errors are the statistical errors in our flux measurements resulting from taking an average of 8 models of the underlying continuum. The systematic uncertainties of 10—15% are far larger than the random errors.

Table 3: Line parameters for the observed H_2 lines.

Transition label	Wavelength (μm)	Energy (Kelvin)	g_j [a]	A 10^{-7} s^{-1}
1-0 S(2)	2.0338	7584	9	3.98
1-0 S(1)	2.1218	6956	21	3.47
1-0 S(0)	2.2235	6471	5	2.53
2-1 S(1)	2.2477	12550	21	4.98

[a] Assumes an ortho/para ratio of 3

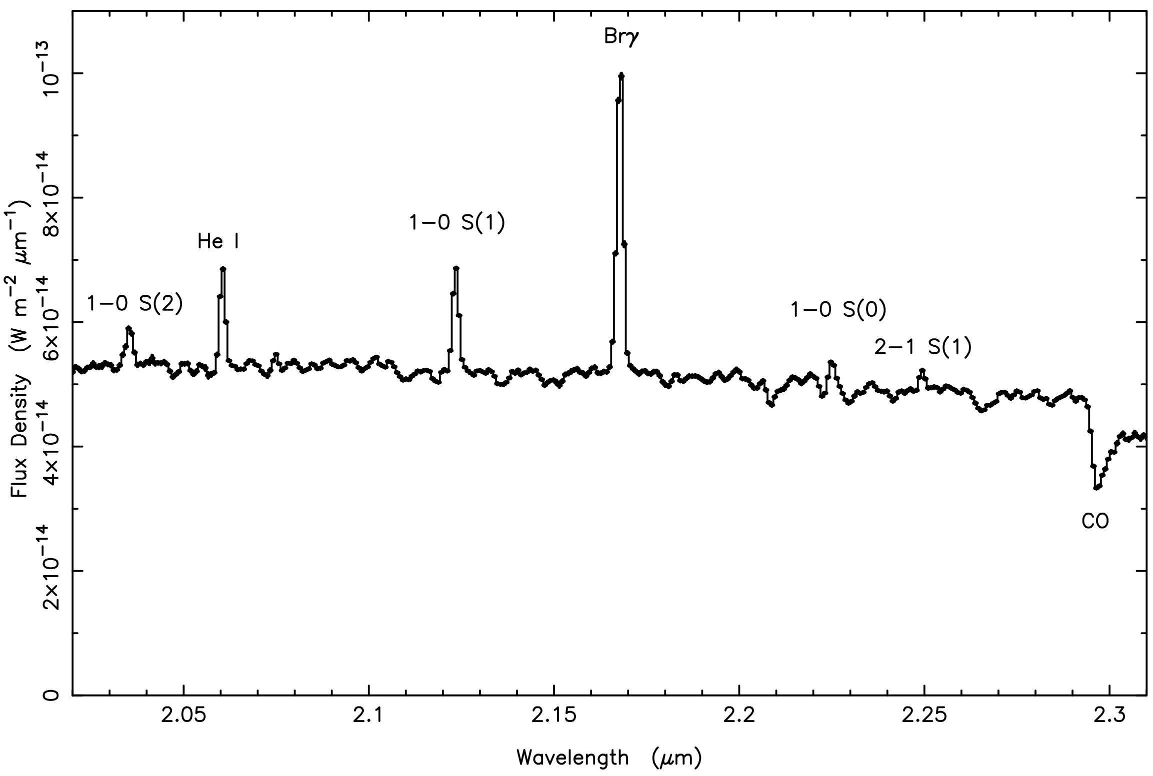

Brγ
1−0 S(2)
He I
1−0 S(1)
1−0 S(0)
2−1 S(1)
CO
Flux Density (W m^{-2} μm^{-1})
Wavelength (μm)
0
2×10^{-14}
4×10^{-14}
6×10^{-14}
8×10^{-14}
10^{-13}
2.05
2.1
2.15
2.2
2.25
2.3

Fig. 1.

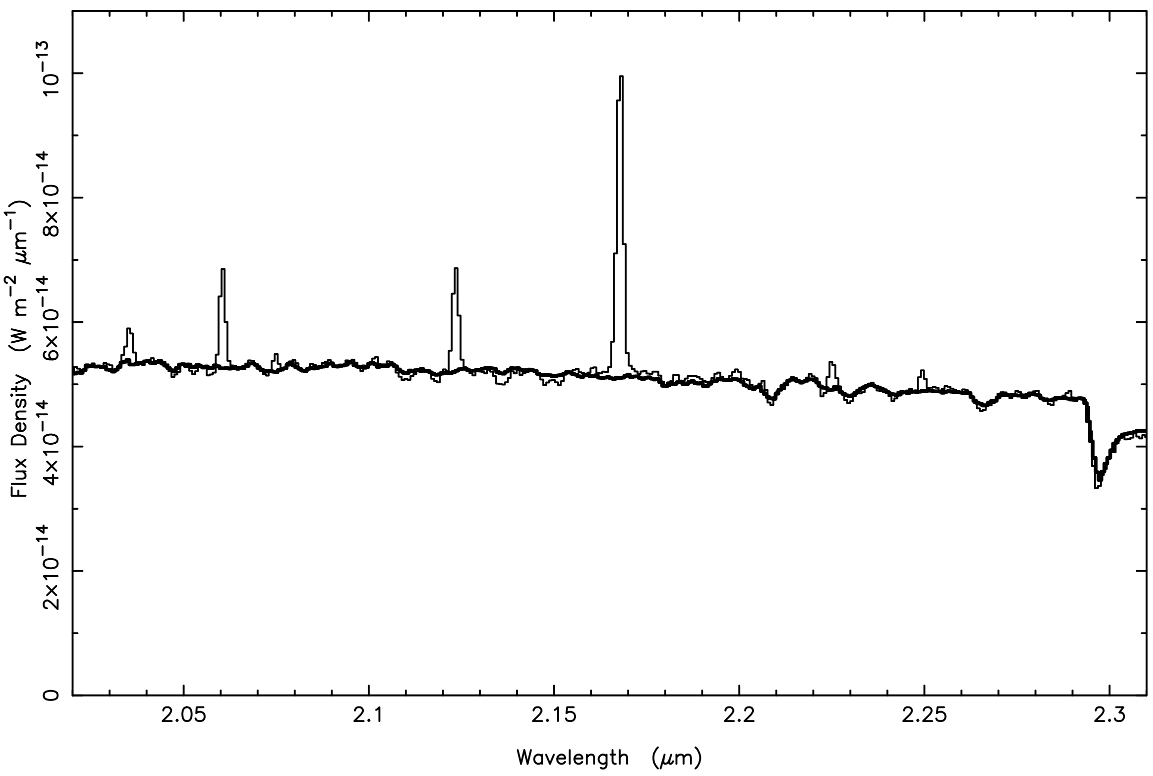

Flux Density (W m^{-2} μm^{-1})
Wavelength (μm)
0
2×10^{-14}
4×10^{-14}
6×10^{-14}
8×10^{-14}
10^{-13}
2.05
2.1
2.15
2.2
2.25
2.3

Fig. 2.

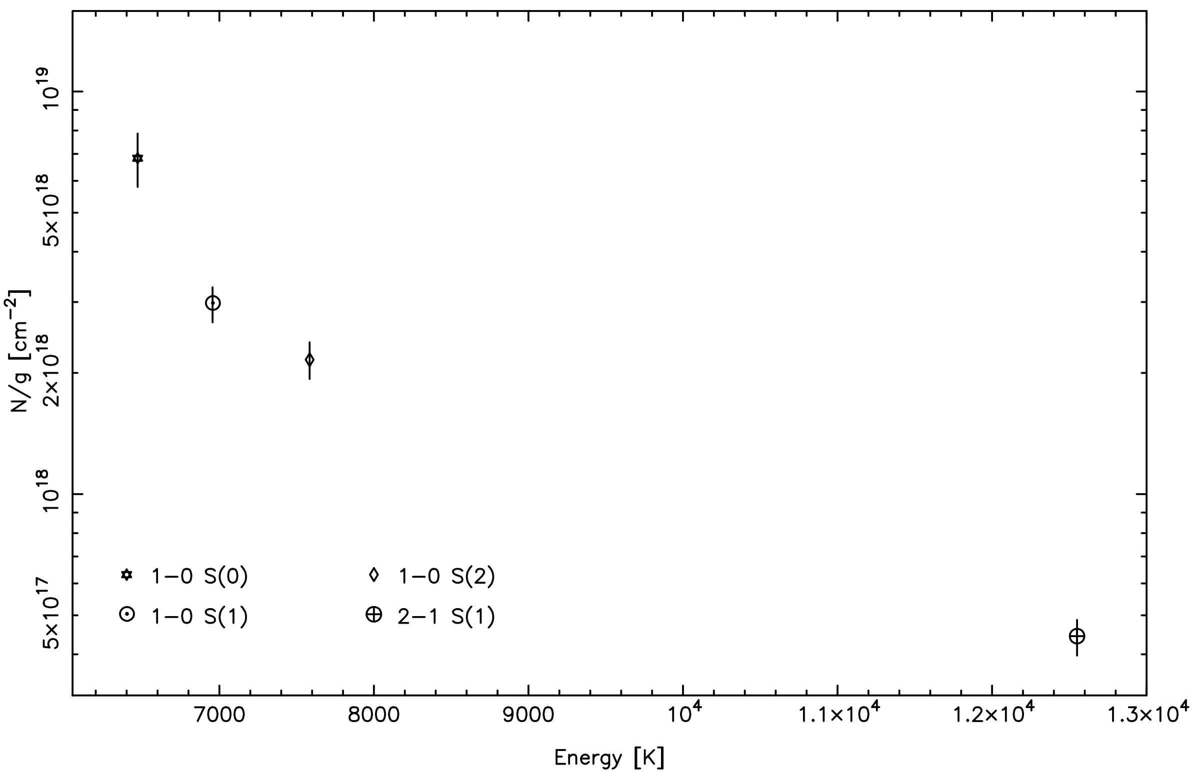

10^{19}
5×10^{18}
N/g [cm^{-2}]
2×10^{18}
10^{18}
5×10^{17}
1−0 S(0)
1−0 S(1)
1−0 S(2)
2−1 S(1)
7000
8000
9000
10^4
1.1×10^4
1.2×10^4
1.3×10^4
Energy [K]

Fig. 3.

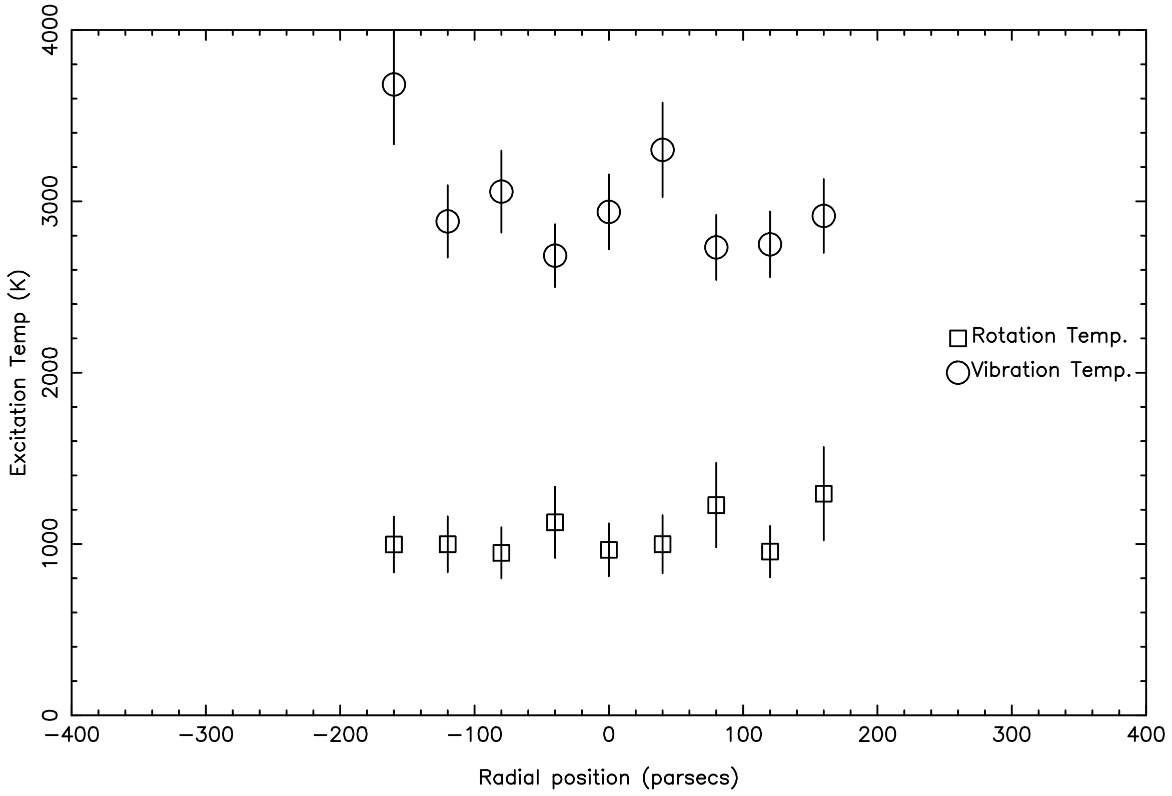

Excitation Temp (K)
Radial position (parsecs)
Rotation Temp.
Vibration Temp.
0
1000
2000
3000
4000
−400
−300
−200
−100
0
100
200
300
400

Fig. 4.

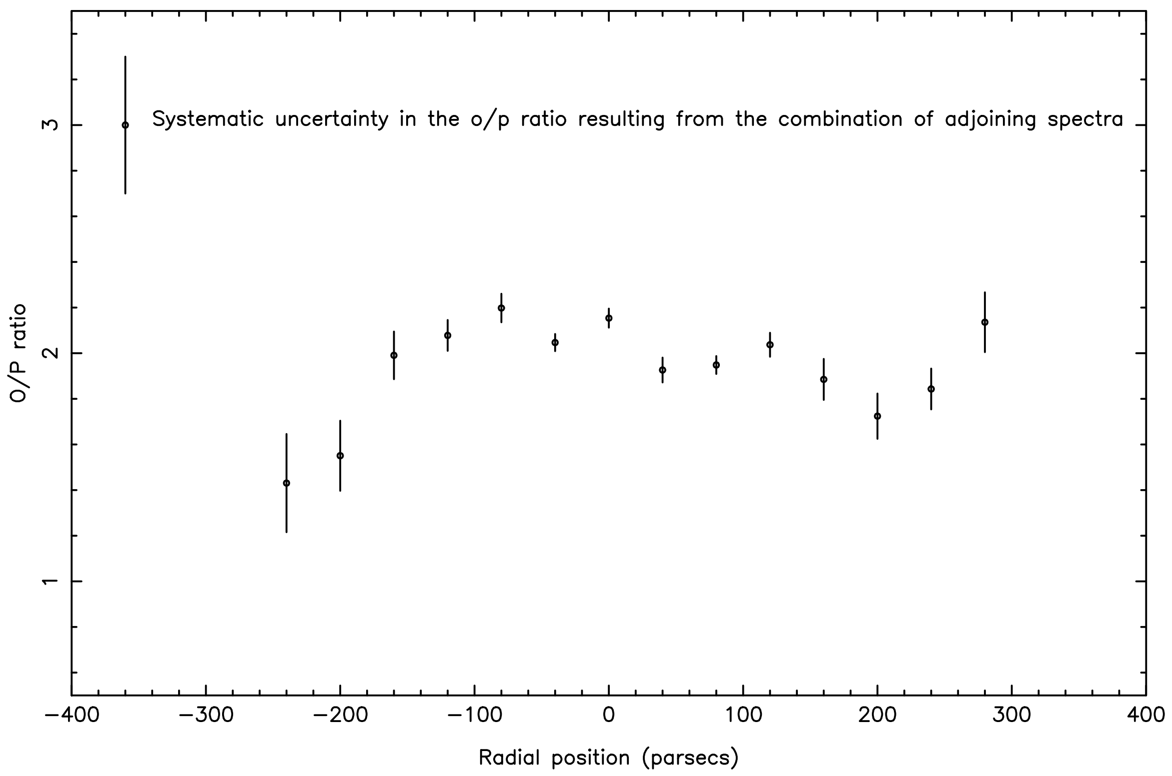
Systematic uncertainty in the o/p ratio resulting from the combination of adjoining spectra
O/P ratio
Radial position (parsecs)
−400
−300
−200
−100
0
100
200
300
400
1
2
3

Fig. 5.

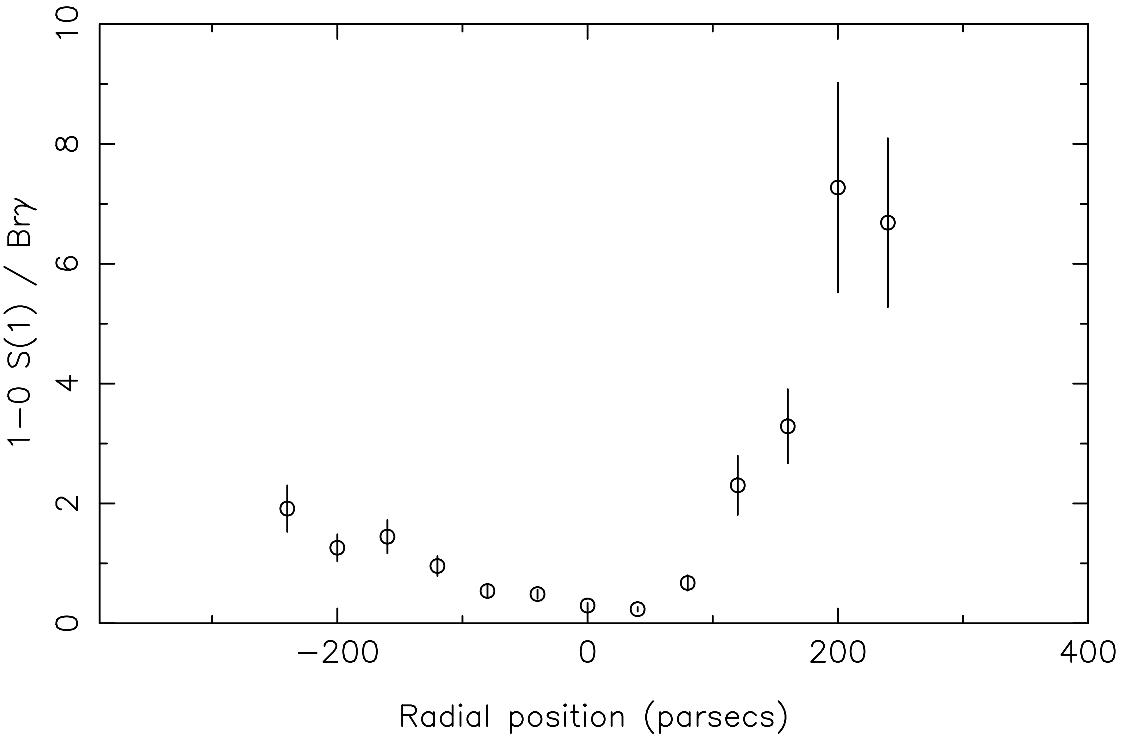

Fig. 6.

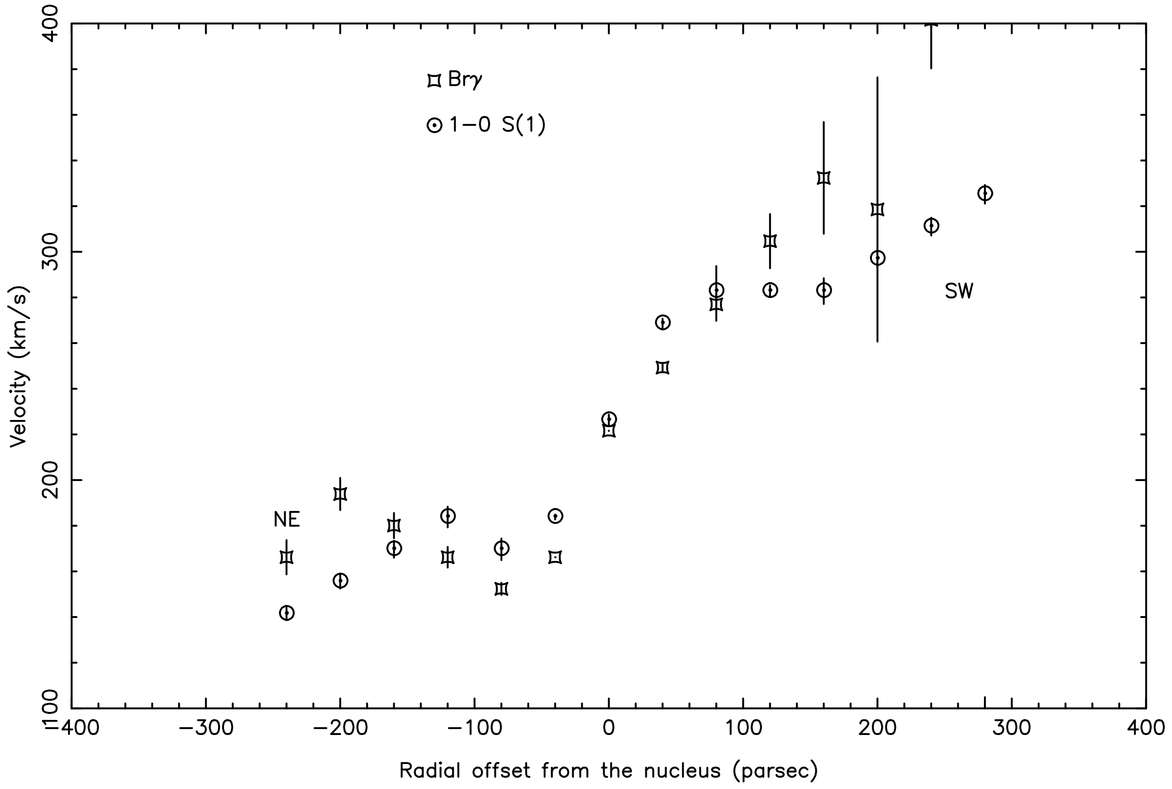
Brγ
1−0 S(1)
NE
SW
Velocity (km/s)
Radial offset from the nucleus (parsec)
100
200
300
400
−400
−300
−200
−100
0
100
200
300
400

Fig. 7.